Supplementary Information

Noncovalent assembly strategy to significantly enhance the iodine adsorption capacity of a Schiff-base macrocycle

Chao Huang*, Shan-Xian He, Rong-Feng Li and Bi-Xue Zhu*

Guizhou Key Laboratory of Macrocyclic and Supramolecular Chemistry, School of Chemistry and Chemical Engineering, Guizhou University, Guiyang 550025, China.

E-mail: chuang1@gzu.edu.cn, bxzhu@gzu.edu.cn

Experimental Section

Materials and measurements

All chemicals and solvents were utilized as received without further purification. Nuclear magnetic resonance (NMR) spectra were recorded in DMSO-d_6 on a JOEL JNM-ECZ400S spectrometer. High-resolution mass spectra (HRMS) were obtained using a Waters Xevo G2-S QTOF spectrometer. Infrared (IR) spectra were recorded using a Bruker VERTEX 70 infrared spectrometer in the range of 4000−400 cm^{-1}. Transmission electron microscopy (TEM) was performed on a JEOL JEM-F200 instrument, and the scanning electron microscope (SEM) was performed on a Zeiss ΣIGMA instrument. Thermogravimetric analyses (TGA) were performed on a TA Q500 analyzer with a temperature range of 25−800 °C under N_2 atmosphere at a heating rate of 10 °C·min^{-1}. X-ray photoelectron spectroscopy (XPS) was performed on a Thermo Scientific K-Alpha instrument. N_2 adsorption isotherms were obtained on a Micromeritics ASAP 2020 HD88 analyzer. A Bruker D8 VENTURE diffractometer with graphite monochromated Mo-Kα radiation (λ = 0.71073 Å) was used to collect the single crystal X-ray diffraction data for macrocycle **M** and diamine **a** at 293(2) K. The OLEX2 program packages were used for the structural solution and full-matrix least-squares refinement. All the non-hydrogen atoms were refined anisotropically and the hydrogen atoms were placed in the calculated positions.

Synthesis

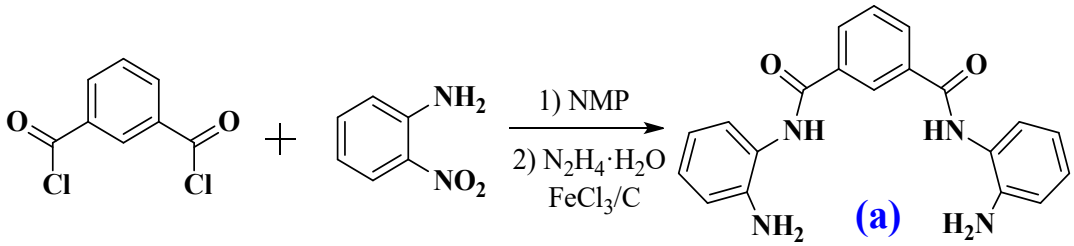

Scheme S1. Synthetic route to diamine **a**

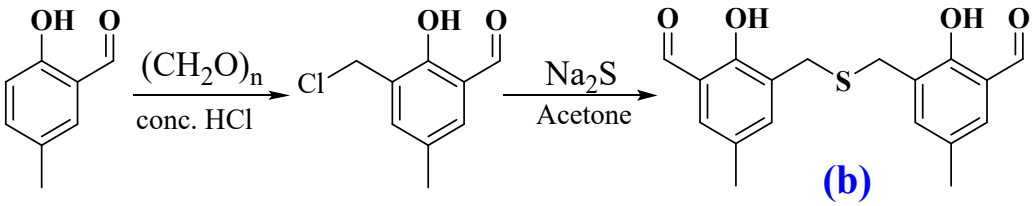

Scheme S2. Synthetic route to dialdehyde **b**

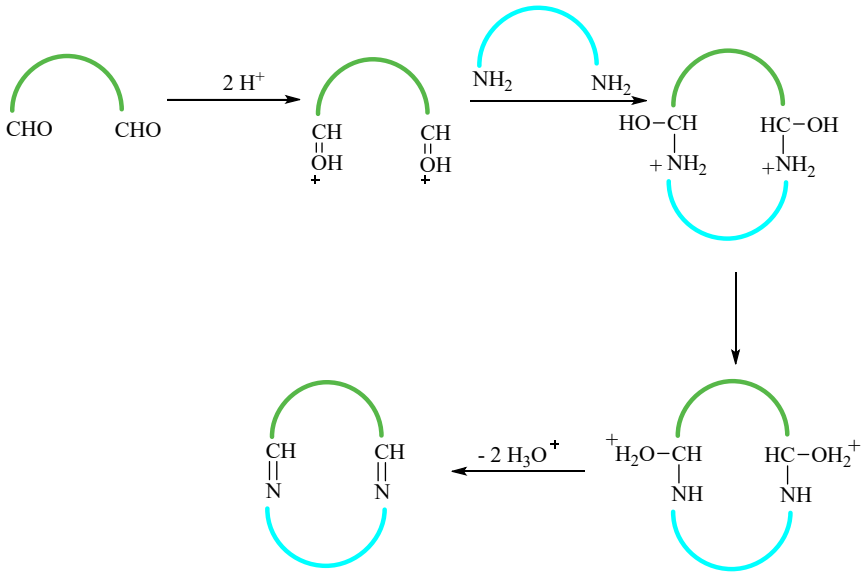

Scheme S3. The formation mechanism of the [1+1] Schiff base macrocycle

Precursor diamine **a** (N^1,N^3-bis(2-aminophenyl)isophthalamide) was synthesized according to the method described in the literature[1]. Isophthaloyl chloride (8.12 g, 0.04 mol) and 2-nitroaniline (11.05 g, 0.08 mol) were dissolved in *N*-methyl-2-pyrrolidone (40 mL), and the solution was stirred for 5 h in an ice-water bath. The resulting mixture was poured into water to give a yellow precipitate, which was subsequently filtered, washed with water, and dried in air to obtain N^1,N^3-bis(2-nitrophenyl)isophthalamide. Yield: 13.82 g (85%). N^1,N^3-bis(2-nitrophenyl)isophthalamide (4.06 g, 0.01 mol), $FeCl_3$ (1.62 g, 0.01 mol), and activated carbon (1.50 g) were mixed in ethanol (100 mL) and heated to boil, then hydrazine hydrate (10 mL) was added dropwise and the reaction was continued to reflux for 8 h. After cooling to room temperature, the mixture was filtered and the solvent was removed under reduced pressure to give a white solid. The crude product was purified by recrystallization in a mixed solution of DMF/MeOH (5:1, *V*/*V*) to obtain N^1,N^3-bis(2-aminophenyl)isophthalamide (**a**). Yield: 2.62 g (76%). ^{1}H NMR (400 MHz, DMSO-d_6): δ 9.74 (s, 2H, −CONH), 8.55 (s, 1H, Ar−H), 8.11 (d, J =

7.6 Hz, 2H, Ar−H), 7.61 (t, J = 8.0 Hz, 1H, Ar−H), 7.15 (d, J = 8.4 Hz, 2H, Ar−H), 6.95 (t, J = 7.6 Hz, 2H, Ar−H), 6.75 (d, J = 8.4 Hz, 2H, Ar−H), 6.57 (t, J = 7.6 Hz, 2H, Ar−H), 4.91 (s, 4H, $-NH_2$).

Dialdehyde **b** 3,3′-thiobis(methyiene)-bis-(5-methyl-salicylaldehyde) was synthesized similarly to our previously reported procedure[2]. To a solution of aldehyde 3-(chloromethyl)-2-hydroxy-5-methylbenzaldehyde (1.84 g, 10.0 mmol) in acetone (50 mL), $Na_2S{\cdot}9H_2O$ (1.20 g, 5.00 mmol) dissolved in distilled water (8 mL) was added. The reaction was stirred at room temperature for 9 h, and then 5% HCl (10 mL) was added. The resulting solution was extracted with dichloromethane (3×50 mL), dried over anhydrous Na_2SO_4, and treated by reduced pressure distillation. The crude product was purified by silica gel chromatography using dichloromethane/petroleum ether (V: V= 1: 1). Yield: 1.17 g (71%). ^{1} H NMR (400 MHz, $CDCl_3$): δ 11.18 (s, 2H, −OH), 9.82 (s, 2H, −CHO), 7.37 (s, 2H, Ar−H), 7.22 (s, 2H, Ar−H), 3.75 (s, 4H, $-CH_2$), 2.29 (s, 6H, $-CH_3$).

Diamine **a** (17.35 mg, 0.05 mmol) and dialdehyde **b** (16.50 mg, 0.05 mmol) were dissolved in methanol (25 mL) separately, and mixed thoroughly in a round-bottomed flask. Then 5 μL of conc. H_2SO_4 was added to the solution. After stirring for 30 min, a light yellow precipitation appeared in the solution, and the reaction was continued at room temperature for 8 h. The resultuing yellow solid was filtered and dried to obtain Schiff-base macrocycle **M**. Yield: 115 mg (72%). ^{1}H NMR (400 MHz, DMSO-d_6) δ (ppm):13.34 (s, 2H, −OH), δ 10.34 (s, 2H, −CONH), 8.88 (s, 2H, CH=N), 8.58 (s, 1H, Ar−H), 8.21 (dd, J_1 = 7.6 Hz, J_2 = 1.6 Hz, 4H, Ar−H), 7.69 (t, J = 8.0 Hz, 1H, Ar−H), 7.53~7.51 (m, 2H, Ar−H), 7.44~7.36 (m, 6H, Ar−H), 7.31 (s, 2H, Ar−H), 7.20 (s, 2H, Ar−H), 3.63 (s, 4H, $-CH_2$), 2.25 (s, 4H, $-CH_3$). ^{13}C NMR (100 MHz, $CDCl_3$) δ (ppm):165.57, 164.02, 156.88, 144.17, 134.99, 134.76, 132.77, 132.05, 131.33, 128.84, 128.80, 128.41, 127.84, 127.61, 127.44, 126.12, 119.26, 119.06, 30.87, 20.41. HRMS: m/z = 641.2209 for $[\mathbf{M}+H]^+$.

The influence of reaction conditions on the morphology of M

The kind of acid catalyst: Diamine **a** (17.35 mg, 0.05 mmol) and dialdehyde **b** (16.50 mg, 0.05 mmol) were dissolved in methanol (25 mL) separately, and mixed thoroughly in a 100 mL round-bottomed flask. The reaction was kept at 25 ℃ under oil bath, then 5 μL of organic acid (formic acid, acetic acid) or 5 μL of inorganic acid (sulfuric acid, hydrochloric acid, nitric acid, phosphoric acid) was added, respectively. After stirring for 8 h, the collected yellow precipitation was tested by SEM.

The amount of sulfuric acid catalyst: Diamine **a** (17.35 mg, 0.05 mmol) and dialdehyde **b** (16.50 mg, 0.05 mmol) were dissolved in methanol (25 mL) separately, and mixed thoroughly in a 100 mL round-bottomed flask. The reaction was kept at 25 ℃ under oil bath, different amounts of sulfuric acid (2 μL, 5 μL, 10 μL, 15 μL) was added as the catalyst. The reaction was continued for 8 h, and the collected yellow precipitation was tested by SEM.

The reaction temperature: Diamine **a** (17.35 mg, 0.05 mmol) and dialdehyde **b** (16.50 mg, 0.05 mmol) were dissolved in methanol (25 mL) separately, and mixed thoroughly in a 100 mL round-bottomed flask. The reaction was kept at 0 °C, 15 °C, 25 °C, 45 °C, and 65 °C under oil bath, respectively, then 5 μL of sulfuric acid was added as the catalyst. The reaction was continued for 8 h, and the collected yellow precipitation was tested by SEM.

The polarity of reaction solvent: Diamine **a** (17.35 mg, 0.05 mmol) and dialdehyde **b** (16.50 mg, 0.05 mmol) were dissolved in different solvents (25 mL) separately, and mixed thoroughly in a 100 mL round-bottomed flask. The reaction was kept at 25 °C and 5 μL of sulfuric acid was added as the catalyst. The reaction was continued for 8 h, and the collected yellow precipitation was tested by SEM.

Monitoring of the assembly process

Diamine **a** (17.35 mg, 0.05 mmol) and dialdehyde **b** (16.50 mg, 0.05 mmol) were dissolved in methanol (25 mL) separately, and mixed thoroughly in a 100 mL round-bottomed flask. The reaction was kept at 25 °C and 5 μL of sulfuric acid was added as the catalyst. The resulted yellow precipitation at different time intervals was tested by

SEM.

Noncovalent assembly of M in different solvents

10 mg of **M** generated in methanol was dissolved in different organic solvents, including DMF, DCM, and DMF/MeOH (*V*/*V*, 1/2). Then the solvents were left for slow evaporation at room temperature. The resulted precipitation was tested by SEM.

Iodine vapor adsorption experiment

50 mg of the three different adsorbents (I, II, and III) was weighed, and placed in a small sample bottle. The mass of the sample bottle containing the adsorbent was recorded, then the sample bottle was put into a larger glass container containing 2.0 g of iodine, and the container was heated to 75 ℃ in an oven to sublime the iodine solid into iodine vapor. After cooling to room temperature, the sample bottle was taken out, and the adsorption capacity was calculated by the following equation:

$$Q = (m_2 - m_1)/m_1 \qquad \text{eq1}$$

Q (g/g) represents the amount of iodine adsorption capacity, and m_1 (g) and m_2 (g) represent the mass of the adsorbent before and after adsorption, respectively.

Adsorption kinetic

The adsorption kinetics of iodine on **III** were investigated by fitting two typical models, pseudo-first-order kinetic and pseudo-second-order kinetic models. The linear forms of the two models can be expressed by the following equations:

$$\ln(q_e - q_t) = -k_1 t + \ln q_e \qquad \text{eq2}$$

$$t/q_t = t/q_e + 1/k_2 q_e^2 \qquad \text{eq3}$$

where q_t (g·g^{-1}) and q_e (g·g^{-1}) denote the amounts of iodine adsorption capacity per g **III** at a specific time t (min) and equilibrium time, respectively. k_1 (min^{-1}) and k_2 (g·g^{-1}·min^{-1}) are the pseudo-first-order and pseudo-second-order rate constants, respectively.

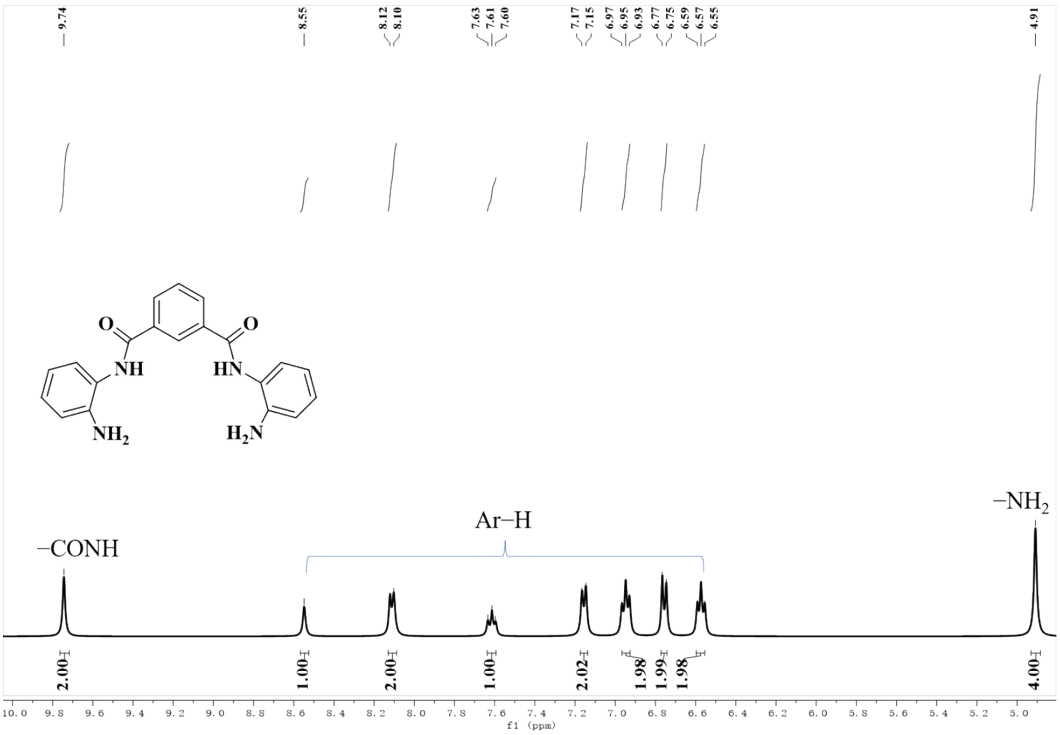

Fig. S1. ^{1}H NMR for diamine **a**

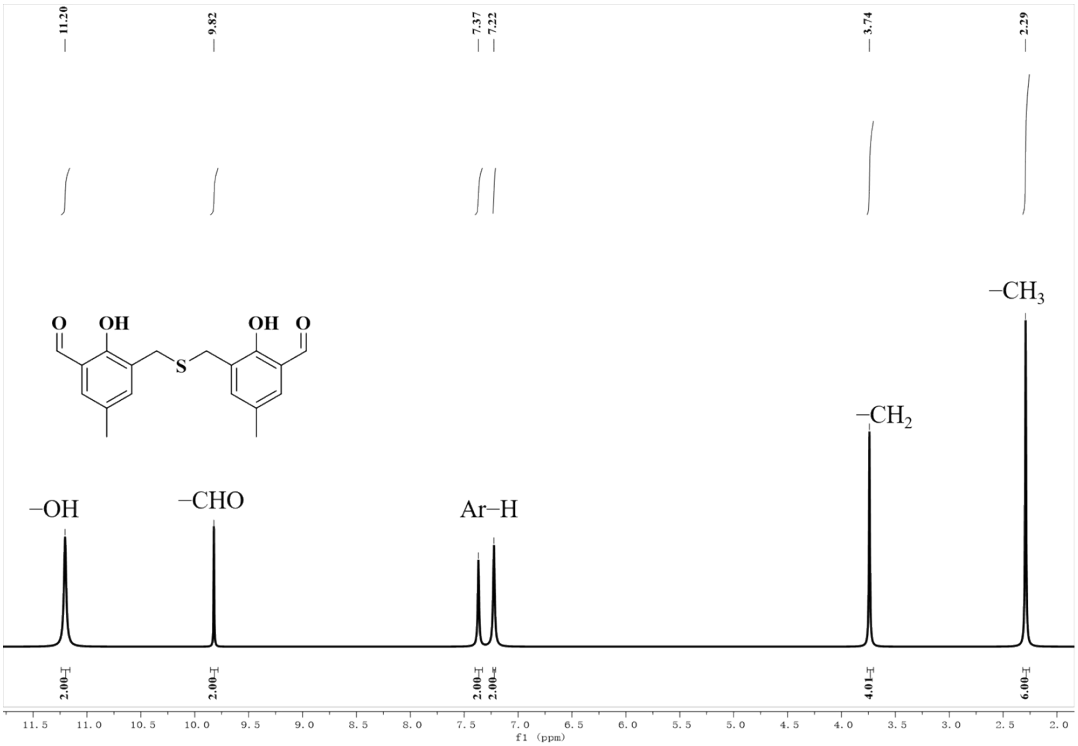

Fig. S2. ^{1}H NMR for dialdehyde **b**

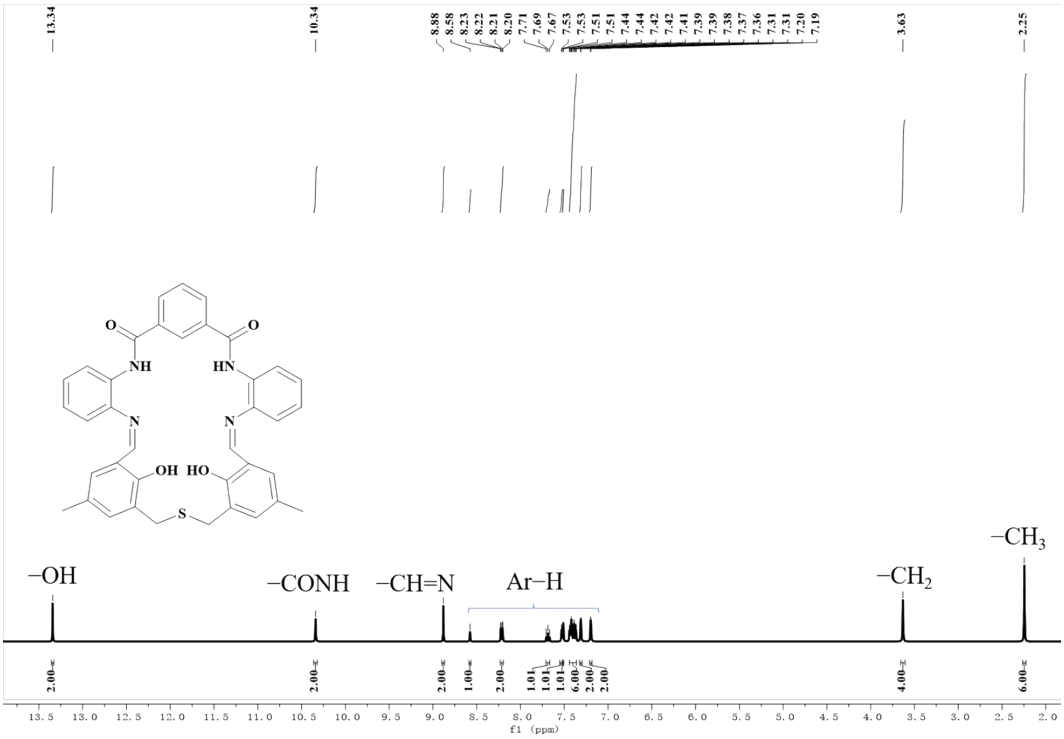

Fig. S3. ^{1}H NMR for **M**

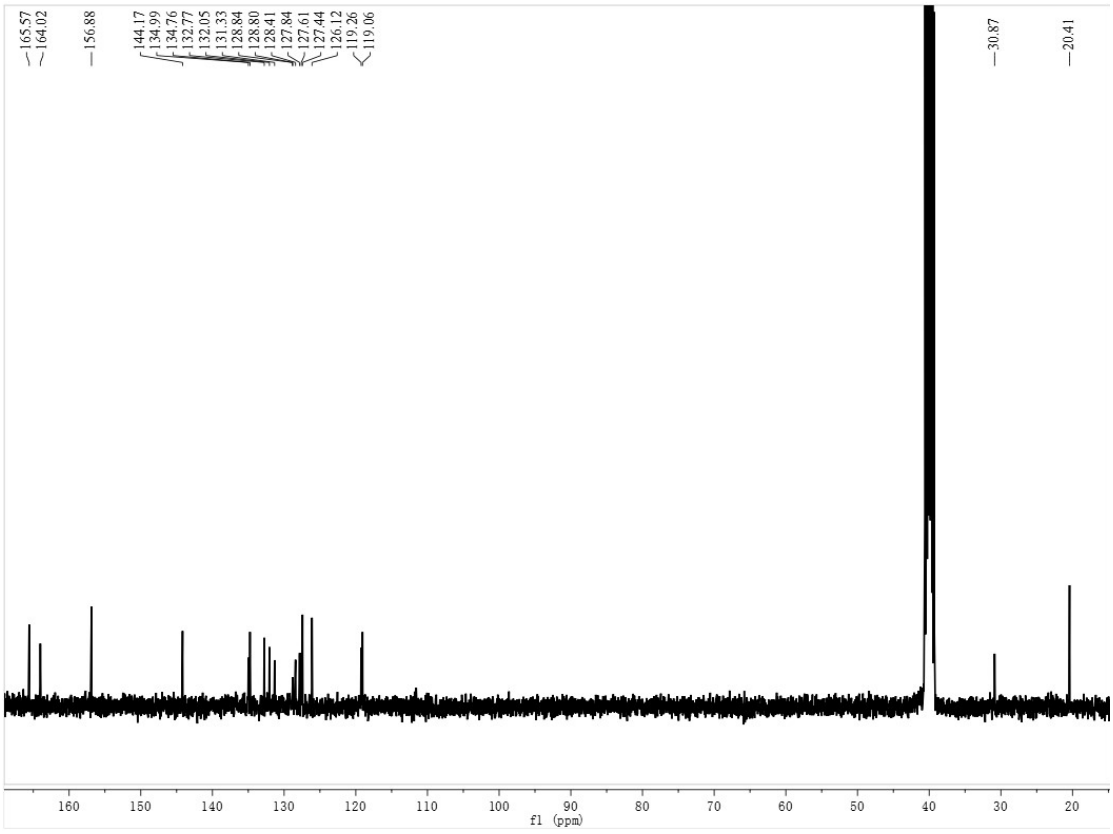

Fig. S4. ^{13}C NMR for **M**

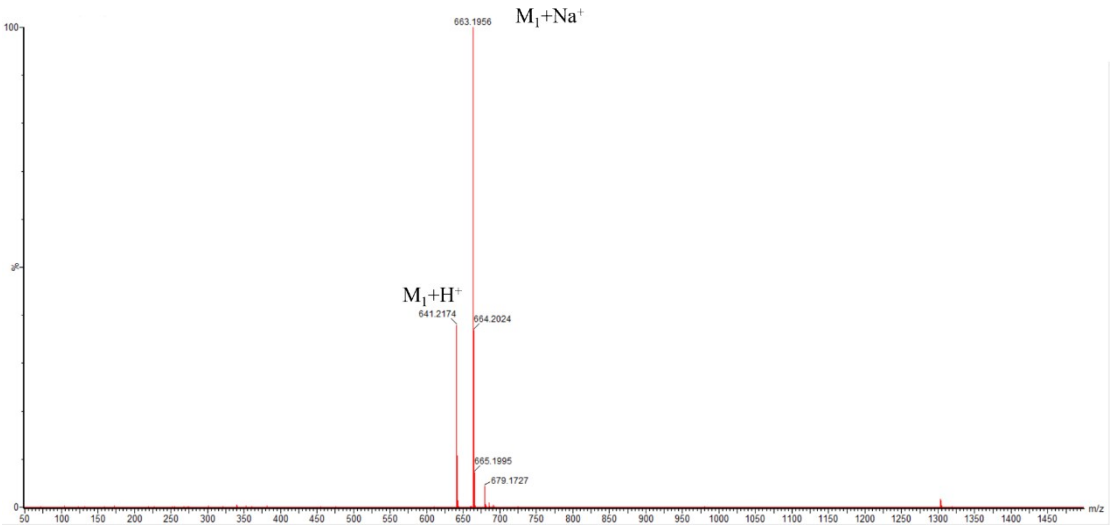

Fig. S5. HRMS for **M**

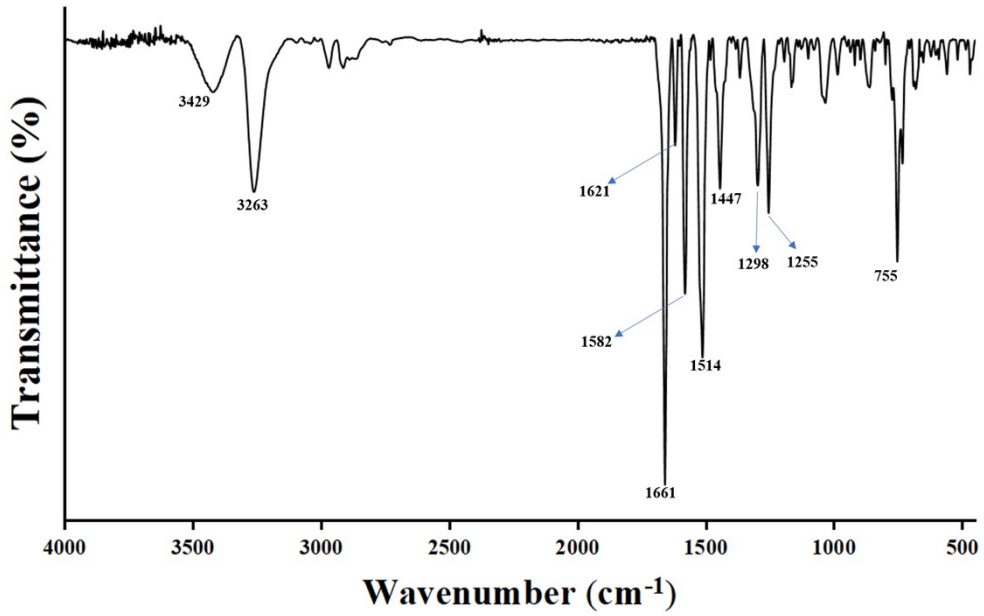

Fig. S6. IR spectrum of **M**

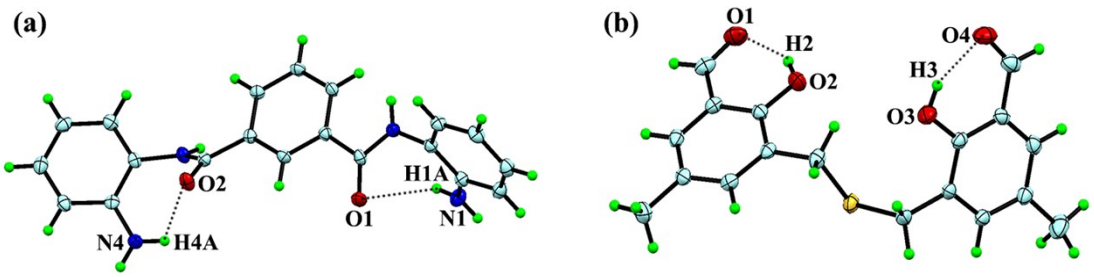

Fig. S7. Crystal structures of diamine **a** (a) and dialdehyde **b** (b).

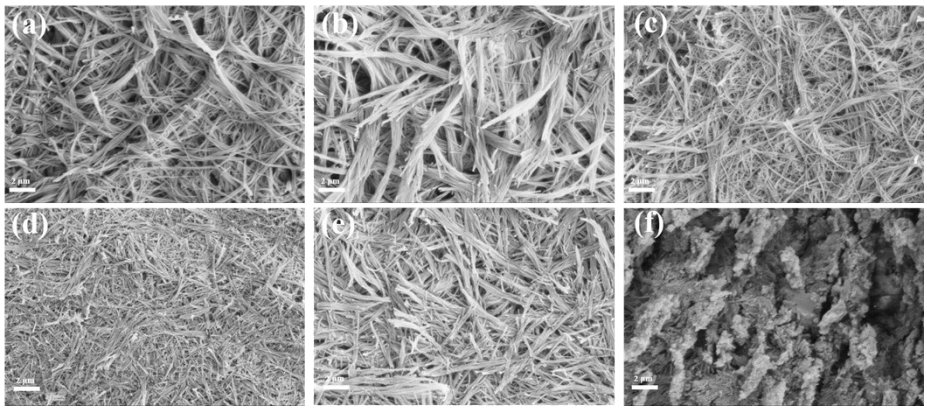

Fig. S8. SEM images of precipitation obtained under different acid catalysts: (a) acetic acid, (b) formic acid, (c) phosphoric acid, (d) nitric acid, (e) sulfuric acid, and (f) hydrochloric acid.

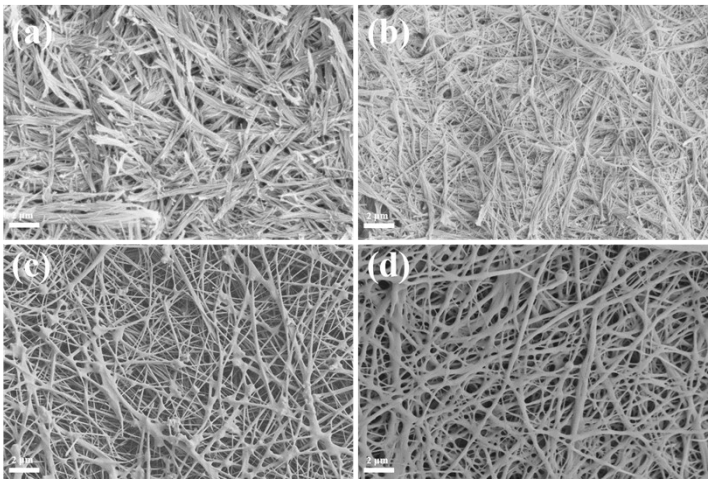

Fig. S9. SEM images of precipitation obtained by adding different amounts of acid: (a) 2 μL, (b) 5 μL, (c) 10 μL, and (d) 15 μL.

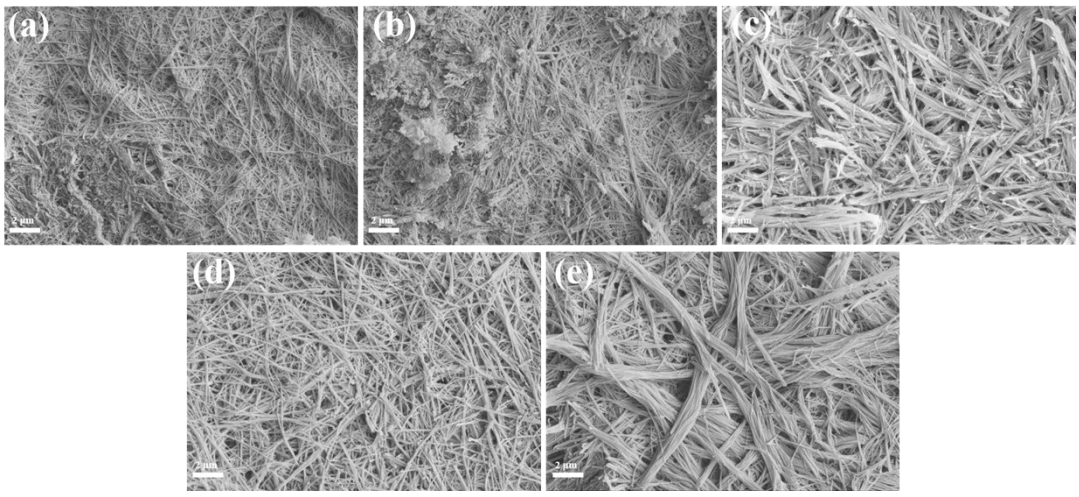

Fig. S10. SEM images of precipitation generated at different reaction temperatures: (a) 0 ℃, (b) 15 ℃, (c) 25 ℃, (d) 45 ℃, and (e) 60 ℃.

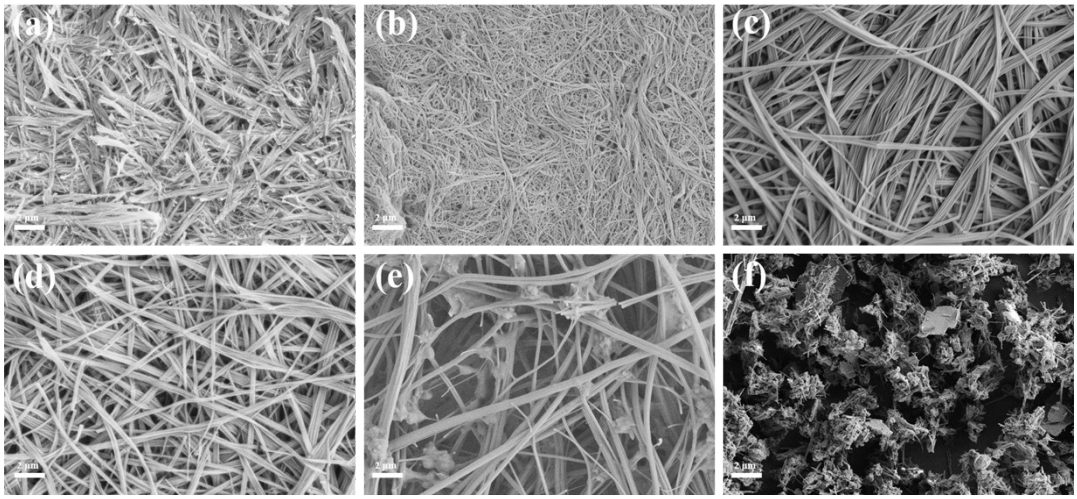

Fig. S11. SEM images of precipitation generated in different polar solvents: (a) MeOH, (b) V_{DCM}: V_{MeOH}= 1:10, (c) V_{DCM}: V_{MeOH} = 1:5, (d) V_{DCM}: V_{MeOH} = 1:2, (e) V_{DCM}: V_{MeOH} = 1:1, and (f) V_{DCM}: V_{MeOH} = 2:1.

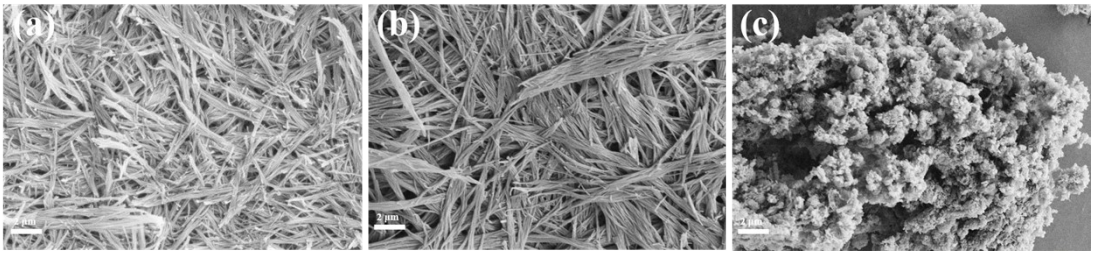

Fig. S12. SEM images of precipitation generated in different polar solvents: (a) MeOH, (b) V_{Water}: V_{MeOH} = 1:10, and (c) V_{Water}: V_{MeOH}= 1:5.

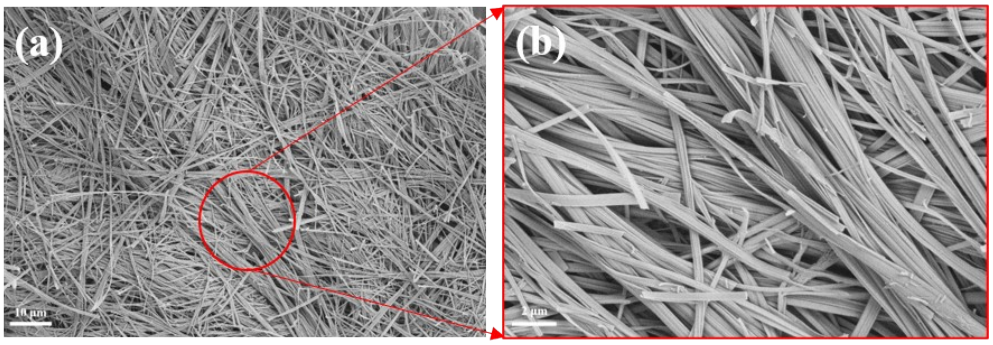

Fig. S13. SEM images of fibers obtained in dichloromethane observed at 1.00 KX (a) and 5.00 KX (b).

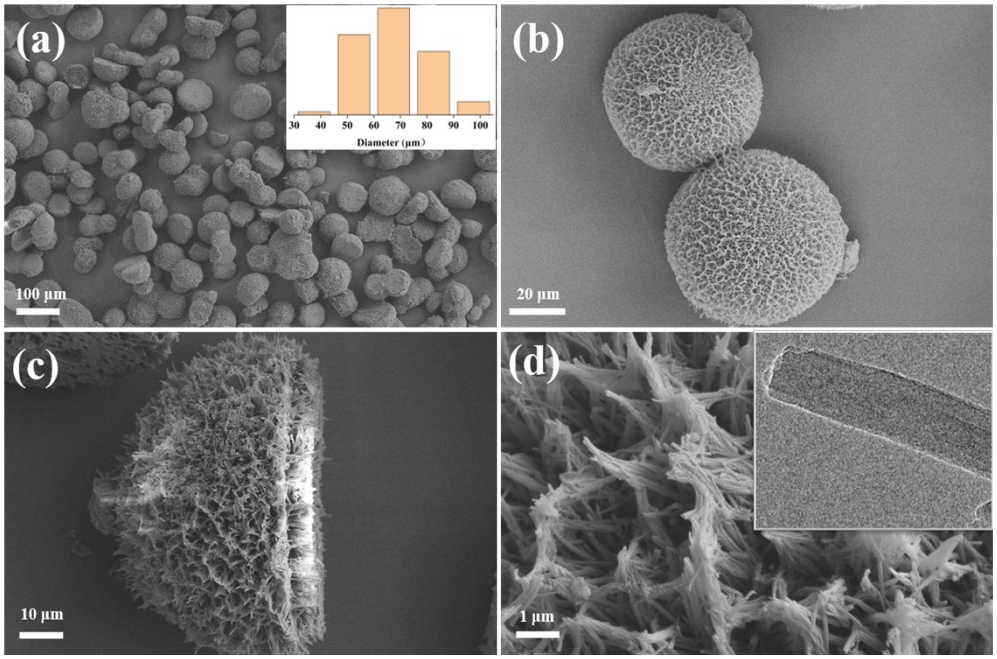

Fig. S14. SEM images of hemispherical particles obtained in DMF: (a) wide-angle view, (b) front view, (c) side view, and (d) the enlarged surface image (illustrated as TEM image).

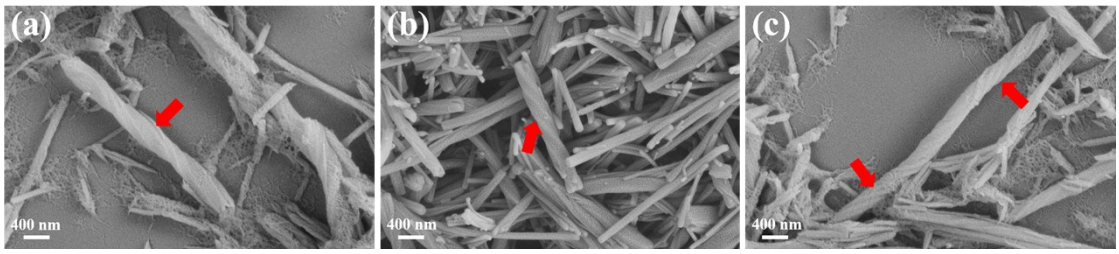

Fig. S15. SEM images of the three forms of rod-like assemblies obtained in DMF/MeOH solution: (a) left-handed helix, (b) right-handed helix, and (c) the coexistence of left- and right-handed helix.

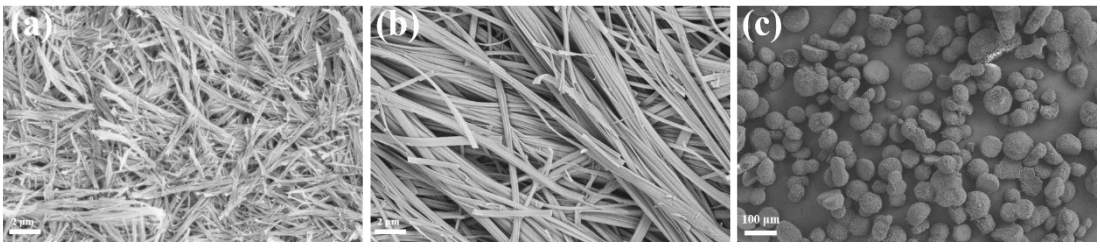

Fig. S16. SEM images of three adsorbents selected for iodine adsorption: (a) **I**, the fiber-shaped precipitation obtained in methanol under sulfuric acid catalysis, (b) **II**, the more slender fibers obtained by slowly evaporating DCM solution containing **M**, and (c) **III**, the hemispherical particles obtained by evaporating DMF solution containing **M**.

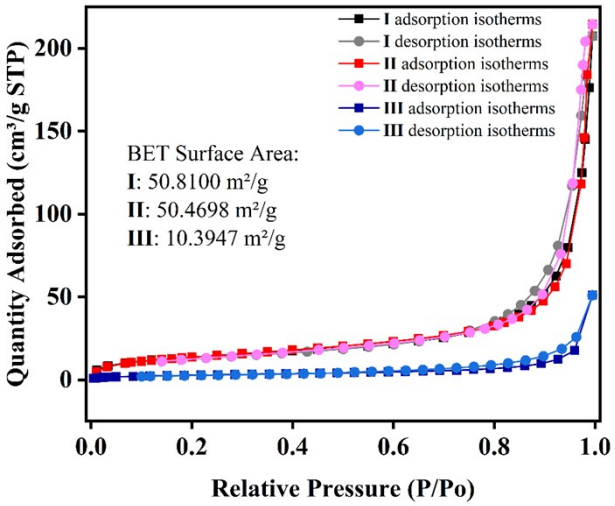

Fig. S17. N_2 adsorption-desorption isotherms of the three adsorbents at 77 K.

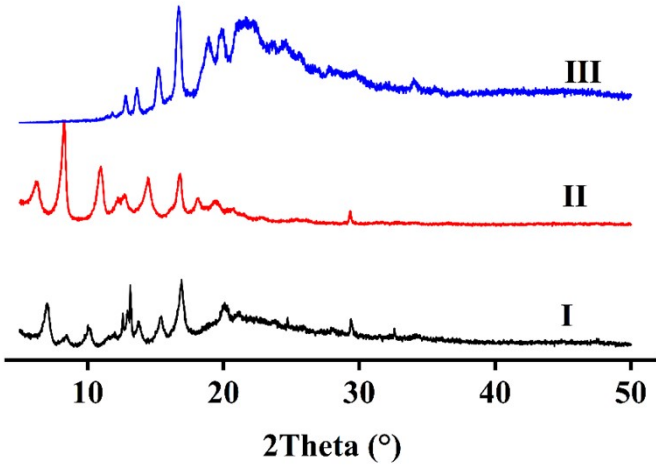

Fig. S18. Comparison of the PXRD patterns for the three adsorbents.

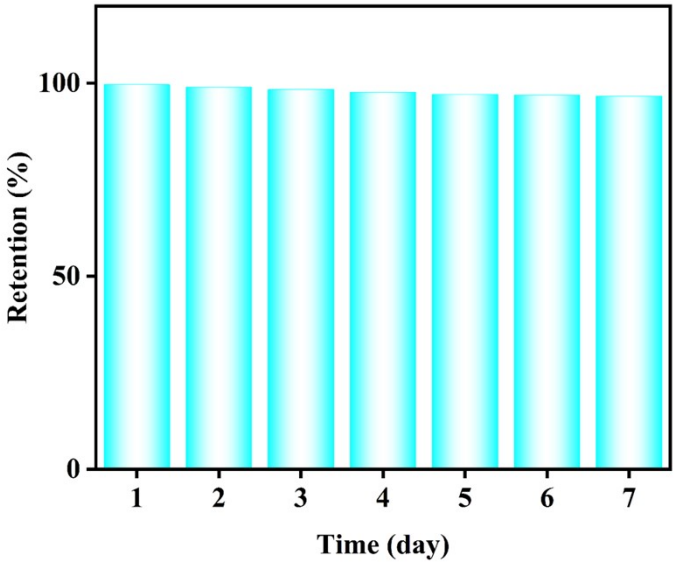

Fig. S19. Iodine retention rate of III@I_2 exposed to air for seven days.

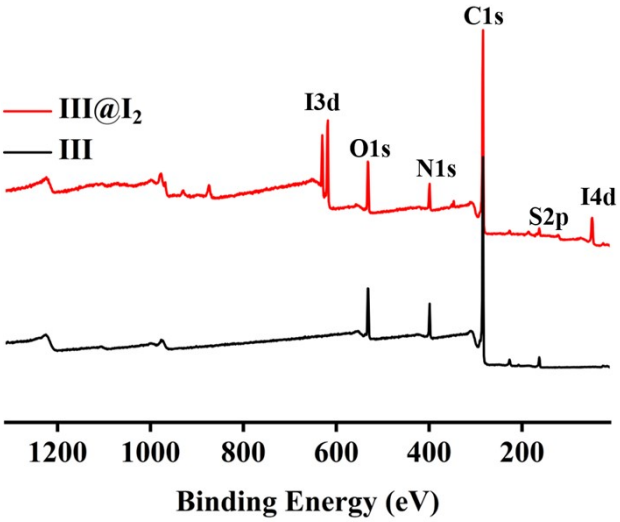

Fig. S20. XPS spectra of adsorbent III before and after iodine adsorption (III@I_2).

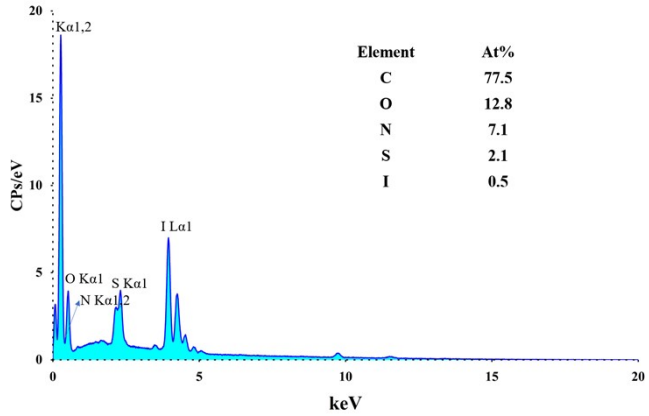

Fig. S21. The EDS diagram of adsorbent III after adsorbing iodine.

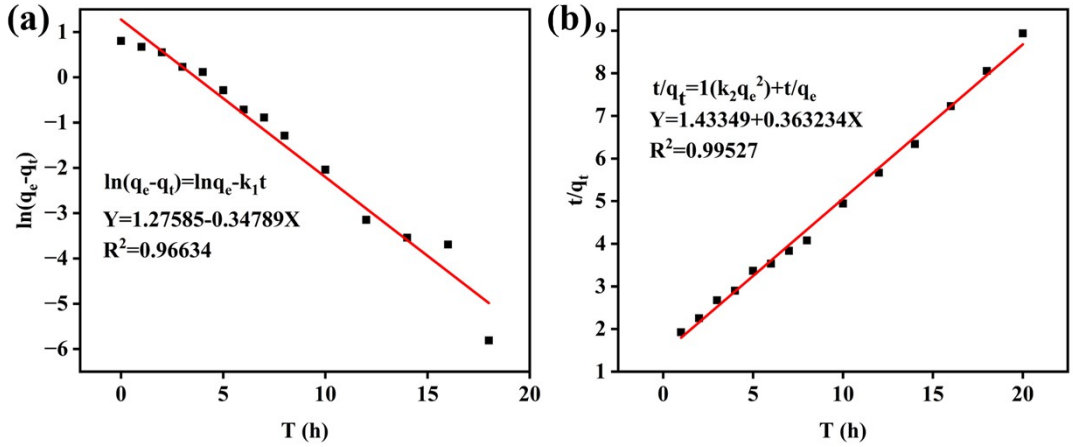

Fig. S22. The kinetic fitting curves by pseudo-first-order model (a) and pseudo-second-order model (b) of **III** for iodine adsorption.

Table S1. Crystal data and structure refinements for **M** and **a**.

Compound	$\mathbf{M}_2\cdot(DMF)_4$	**a**
CCDC	2413994	2325855
Empirical formula	$C_{88}H_{92}N_{12}O_{12}S_2$	$C_{20}H_{18}N_4O_2$
Formula weight	1573.85	346.38
Crystal system	orthorhombic	monoclinic
Space group	*Pbca*	$P2_1/c$
a / (Å)	29.98(4)	5.392(3)
b / (Å)	14.09(3)	35.07(2)
c / (Å)	39.28(3)	8.645(6)
α / (°)	90	90
β / (°)	90	93.24(2)
γ / (°)	90	90
V / (Å^3)	16589(41)	1632.4(18)
Z	8	4
D_c / (g·cm^{-3})	1.260	1.409
θ range / (°)	2.050~24.500	2.323~25.999
μ / mm^{-1}	0.133	0.094
F (000)	6656	728
Reflections collected	128007	22865
Independent reflections	13797	3212
Observed reflections ($I>2\sigma(I)$)	8884	1812
Number of parameters	924	235
Goodness-of-fit on F^2	1.120	1.047
Final R indices ($I>2\sigma(I)$)	$R_1 = 0.1382$, $wR_2 = 0.2217$,	$R_1 = 0.0727$, $wR_2 = 0.1704$
R indices (all data)	$R_1 = 0.2063$, $wR_2 = 0.2450$	$R_1 = 0.1393$, $wR_2 = 0.2041$
Peak and hole (e Å^{-3})	0.814 and -0.559	0.444 and -0.316

Table S2. Hydrogen bond distances (Å) and angles (°) for **M** and **a**.

	D−H···A	D−H(Å)	H···A(Å)	D···A(Å)	∠DHA
M	N1−H1···O2	0.86	2.29	3.133(10)	167
	N2−H2···O9$^{\#1}$	0.86	2.09	2.879(10)	153
	O3−H3···N7	0.82	1.92	2.646(10)	148
	O4−H4···N10	0.82	1.85	2.574(9)	146
	O7−H7···N3	0.82	1.90	2.620(9)	146
	O8−H8···N4	0.82	1.88	2.602(10)	147
	O8−H8A···O11	0.86	2.19	2.933(11)	144
	N9−H9···O12	0.86	2.06	2.879(10)	158
	C5−H5···O11	0.93	2.44	3.272 (11)	148
	C26−H26···O6$^{\#2}$	0.93	2.54	3.412(10)	156
	C31−H31···O1$^{\#3}$	0.93	2.48	3.377(11)	162
	C39−H39···N7	0.93	2.56	3.453(10)	160
	C43−H43···O9$^{\#1}$	0.93	2.36	3.256(10)	162
	C74−H74···O12$^{\#4}$	0.93	2.55	3.448(10)	167
	C78−H78B···S1	0.96	2.86	3.803(14)	167
a	N1−H1A···O1	0.86	2.53	2.942(5)	110
	N1−H1A···O2$^{\#1}$	0.86	2.39	3.149(5)	148
	N3−H3···O1$^{\#1}$	0.86	2.49	3.340(5)	171
	N4−H4A··O2	0.86	2.47	2.894(5)	111
	N4−H4B···N1	0.86	2.40	3.243(5)	165
	C9−H9···O2$^{\#2}$	0.93	2.46	3.344(5)	159

$^{\#1}$:1/2-*x*, 1/2+*y, z*; $^{\#2}$:1-*x*, 1/2+*y*, 1/2-*z*; $^{\#3}$:3/2-*x*, 1/2+*y*, *z*; $^{\#4}$:1-*x*, 3-*y*, 1-*z* for **M**.

$^{\#1}$: *x*, 3/2-*y*, -1/2+*z*; $^{\#2}$: -1+*x*, 3/2-*y*, -1/2+*z* for **a**.

`

Table S3. Comparison of saturated iodine uptakes for the reported adsorbents.

Adsorbents	Iodine uptake ($g \cdot g^{-1}$)	Reference
Co-CP	3.54	3
TTA-DMTP-COF	2.59	4
PAF-P	2.29	5
M-III	2.23	This work
HBP-PyTS	2.20	6
P5–P5I	2.13	7
Ni^{2+}-based cluster	2.08	8
Cu^0_89 wt%@h–BN	1.82	9
SBA-15	1.78	10
Q[8]-(4-AP)	1.74	11
CMPs-1@PU	1.63	12
10BrP5-TPPA	1.57	13
CAU-1	1.28	14
Cu/Al_2O_3-Pal aerogel	1.12	15
Ag-Mxene(Ag-$Ti_3C_2T_x$)	0.95	16
M-II	0.65	This work
UiO-66_NH_2/ZrCSx-*f*	0.32	17
M-I	0.26	This work

Table S4. The parameters of the two kinds of kinetic models for III.

Model	q_e(exp) ($g.g^{-1}$)	q_e ($g.g^{-1}$)	k	R^2
pseudo-first-order	2.23	2.75	0.092 min^{-1}	0.966
pseudo-second-order		3.58	0.348 $g.g^{-1}.min^{-1}$	0.995

References

1. C. Huang, H.-Q. Tian, R.-F. Li, Y. Xiong, T. Jiang, D.-M. Chen and B.-X. Zhu, *Inorg. Chem.*, 2022, **61**, 19512-19523.
2. H.-H. Yu, S.-X. He, J.-H. Lu, C. Huang, D.-M. Chen and B.-X. Zhu, *Inorg. Chim. Acta*, 2023, **557**, 121713.
3. J. Suebphanpho, P. Jearanaiwiwat, K. Chainok and J. Boonmak, *Chem. Asian J.*, 2025, e202401532.
4. W.-Z. She, Q.-L. Wen, H.-C. Zhang, J.-Z. Liu, R. S. Li, J. Ling and Q. Cao, *ACS Appl. Nano Mater.*, 2023, **6**, 18177-18187.
5. Z. Li, X. Liu, T. Meng, Y. Peng, H. Lei, M. Guo, S. Chaleawlert-umpon, H. Su, C. Yang and L. Li, *Colloids Surf., A,* 2025, **710**, 136216.
6. W. Xu, C. Gao, Y. Zhang, M. Sun, H. Qiu and J. Chen, *Sep. Purif. Technol.*, 2025, **364**, 132495.
7. Y. Chen, M.-K. Yang, S.-X. Li, S.-L. Zhou, C.-N. Hu, Y.-H. Yang and L.-J. Yang, *ACS Appl. Mater. Interfaces*, 2025, **17**, 8382-8393.
8. J. Qiu, L. Tang, Z. Nan, L. Liu, Q. Li, W. Wang, Z. Zhuo, D. Zhang, Y. Huang and L. Zhang, *Molecules*, 2025, **30**, 989.
9. T.-S. Chee, S. Lee, W. Jeong and H. J. Ryu, *Chem. Eng. J.,* 2025, **507**, 160201.
10. L. Chen, W. Fan, X. He, Y. Li, Z. Zhang, L. Han, B. Liu, H. Dan and Y. Ding, *Sep. Purif. Technol.*, 2025, **364**, 132456.
11. Y. Lu, Z. Yu, T. Zhang, D. Pan, J. Dai, Q. Li, Z. Tao and X. Xiao, *Small*, 2024, **20**, 2308175.
12. A. Yi, Y. Zhang, Q. Chen, C. Guo, Y. Jing, H. Sun, R. Jiao, J. Li, Z. Zhu and A. Li, *Surf. Interfaces*, 2025, **63**, 106362.
13. C.-L. Song, M.-H. Li, G. Wu, C. Wang and Y.-W. Yang, *ACS Mater. Lett.*, 2025,

7, 1905-1913.

14. G. Chen, L. Wu, Z. Wang, R. Liu, C. Tan, Y. Tan, Y. Liu, M. He, H. Zhang, Y. Huang, J. Zhu, T. Duan and L. Zhu, *Chem. Eng. J.*, 2025, **507**, 160829.
15. X.-Y. Zhou, H.-R. Jin, A.-T. Gu, K.-W. Chen, Y.-J. Liu, S. Yun, P. Mao, J. Chen and Y. Yang, *Microporous Mesoporous Mater.*, 2024, **366**, 112963.
16. K. Eisawi, E. Loni, S. Chong, M. Liezers, M. Tang, K. S. Brinkman, B. J. Riley and M. Naguib, *Adv. Mater. Interfaces*, 2025, **12**, 2500011.
17. N. Hammi, M. Boundor, S. Chen, N. Couzon, A. El Kadib, A. Ferri, F. Pourpoint, T. Loiseau, C. Volkringer, S. Royer and J. Dhainaut, *ACS Appl. Mater. Interfaces*, 2025, **17**, 3952-3961.